Applied Clay Science 124–125 (2016) 219–226

Contents lists available at ScienceDirect

Applied Clay Science

journal homepage: www.elsevier.com/locate/clay

Note

How to face the new industrial challenge of compatible, sustainable brick production: Study of various types of commercially available bricks

Chiara Coletti [a,b,*], Giuseppe Cultrone [b], Lara Maritan [a], Claudio Mazzoli [a]

[a] Department of Geosciences, Padova University, Via G. Gradenigo 6, 35131 Padova, Italy
[b] Department of Mineralogy and Petrology, Faculty of Science, Granada University, Avda. Fuentenueva s/n, 18002 Granada, Spain

ARTICLE INFO

Article history:
Received 21 October 2015
Received in revised form 11 February 2016
Accepted 12 February 2016
Available online 28 February 2016

Keywords:
Clay bricks
Firing temperature
Physical–mechanical properties
Petrography
Pore system
Sustainable construction materials

ABSTRACT

In the view of a sustainable production responding to the important challenges to which industrial research is currently facing, this research is addressed to define the more appropriate brick types, among those here studied, in terms of mechanical resistance and durability, as well as the esthetic qualities. More in detail, five industrial bricks, produced with three types of clay and fired at four temperatures (600, 950, 980, 1050 °C), were analysed with a combined multianalytical approach to determine relationships between mineralogical-textural and physical-mechanical properties and decay behavior. Samples fired at 1050 °C show more complete mineralogical evolution and have the best mechanical resistance, but are the most sensitive to the water absorption. Instead, samples fired at the lowest temperature (600 °C) have the best pore interconnections and the lowest coefficient of capillarity, however, the absence of new silicates and melting make them the weakest under load and decay tests. Lastly, bricks produced at firing temperatures of 950 °C and 980 °C generally show intermediate behavior. These results indicate how bricks produced form the same or similar mix design and fired at different temperatures show different reactions to decay and mechanical resistance, allowing the industry to identify the limit of applicability of these materials in various contexts.

© 2016 Elsevier B.V. All rights reserved.

1. Introduction

Brick, a ceramic product used as building material since ancient times, is still valued for its easy availability of georesources, resistance to loading and environmental stress, and its esthetic quality. During firing, the raw materials, generally a mixture of a body of clay minerals and predetermined fractions of silt and sand (temper), is transformed into a new artificial material in which mineralogical changes occur, similar to those which developed during pyrometamorphism; as regards microstructure, new porosity develops and melts form (Riccardi et al., 1999; Aras, 2004; Cultrone et al., 2004). Many works have been published on case studies of historic interest, with specific focus on the mineralogy and texture of fired samples (Cardiano et al., 2004; Cultrone et al., 2005a), the provenance of raw materials (López-Arce et al., 2003; Maritan et al., 2005) and firing conditions (Setti et al., 2012), as well as on the phase transformations during firing of artificial samples (Dondi et al., 1998; Duminuco et al., 1998; Riccardi et al., 1999; Elert et al., 2003; Aras, 2004; Cultrone et al., 2004; Cultrone et al., 2005b; Maritan et al., 2006; Nodari et al., 2007; Fabbri et al., 2014) and have greatly contributed to our knowledge of the physical and mechanical changes according to raw material composition and firing temperature (Cultrone et al., 2001b; Carretero et al., 2002; De Bonis et al., 2014). Porosity and decay have also been investigated, to evaluate the parameters controlling durability, since bricks, like any other construction material, are affected by various and sometimes combined deterioration phenomena (Valluzzi et al., 2002; Valluzzi et al., 2005; Anzani et al., 2010). Examples are interactions with other materials nearby (Larbi, 2004; Cultrone et al., 2007), environmental conditions, and the presence of soluble salts (Cultrone et al., 2000; Rodriguez-Navarro et al., 2000; Benavente et al., 2003) or ice (Grossi et al., 2007a; Ducman et al., 2011). Nevertheless, although extensive studies on ceramic materials have been carried out, little research has focused on the real needs of brick industries. This work aims to close this gap, in collaboration with the personnel of a brick factory and focusing on actual requirements in industrial research, i.e., the creation of new mixes for specific situations (e.g., restoration of historical buildings) and the promotion of sustainable solutions in terms of saving resources and energy. Replacing some particular types of bricks in a damaged historic structure requires caution in operating in a way which is mechanically and chemically compatible with the undamaged materials and in preserving the overall original appearance (Cardiano et al., 2004). The brick industry is also encouraged to ensure quality, to improve eco-friendly brick production, and to optimize firing conditions, while maintaining the characteristics which make brick a traditional material, in which our cultural identity can be recognized (Cultrone and Sebastián, 2009; Eliche-Quesada et al., 2012; Zhang, 2013; Monteiro and Fontes Vieria, 2014).

* Corresponding author at: Department of Geosciences, Padova University, Via G. Gradenigo 6, 35131 Padova, Italy.
E-mail address: chiara.coletti@studenti.unipd.it (C. Coletti).

http://dx.doi.org/10.1016/j.clay.2016.02.014
0169-1317/© 2016 Elsevier B.V. All rights reserved.

Table 1
Labels of raw materials and bricks and their maximum firing temperatures.

Clay	Additive	Brick type	Firing temperature (°C)
LG	-	GP	1050
	Hausmannite	N	1050
LRSS	-	RSS	950
	-	R6	600
LRS	-	RS	980

Compared with natural stone, brick has the advantage that its technical and esthetic qualities can be modified by changing the composition of raw materials and/or firing conditions to obtain certain properties, depending on the position or function the brick is required to carry out in a given place and environment. Identifying new mix designs for use in historic and modern constructions is a challenge of prime interest for restorers and builders. This work develops a valid multianalytical approach to study the properties of bricks, starting from five different types, four already on the market, in order to have a solid basis on which to tackle the actual industrial challenge of identifying methods and criteria to introduce green solutions to the market and ensure a leadership industry promoting excellence and innovation. Awareness of the close connections among mineralogy, porosity and physical properties can lead to improved quality in the brick industry as a whole, allowing us to take the next steps toward sustainable, compatible production and introducing new materials adapted to particular cultural and environmental contexts.

2. Materials and methods

Three types of clay raw materials largely adopted from the brick factory SanMarco-Terreal (Noale, Veneto, Italy) were studied: LG (*Laminato Giallo*, i.e. "Yellow Laminated"), LRSS (*Laminato Rosso*, "Red Laminated") and LRS (*Laminato Rosa*, "Pink Laminated"). From these clays, five types of bricks (GP, N, RSS, RS and R6) were prepared by SanMarco-Terreal according to the "soft mud" method: GP (*Giallo Paglierino*, i.e., "Straw Yellow") obtained with LG clay fired at 1050 °C; N (*Nero*, "Black") produced with LG clay with the addition of 15 wt% of hausmannite powder (Mn_3O_4), to obtain a dark gray product, and fired at 1050 °C; RSS (*Rosso*, "Red") and R6 (*Rosso600*, "Red600") prepared with LRSS clay fired at 950 and 600 °C, respectively; RS (*Rosato*, "Pink") obtained by LRS clay fired at 980 °C (Table 1). Samples were fired in a tunnel kiln, with the following temperature curve: heated to maximum temperature in 1-h and left at maximum temperature for 1-h (soaking time).

Both clay materials and fired bricks (two specimens per type of bricks) were characterized using a multianalytical approach: type of instruments and instrumental setting for each technique adopted are described in Table S1. Equations used to calculate the physical parameters from instrumental data are reported in Table S2.

Color coordinates (L*, a* and b*) were determined for both clay materials and fired bricks (dry and wet) and color difference ΔE calculated for each brick (UNE EN 15886, 2011). The mineralogical composition of raw materials and bricks was determined from X-ray Powder Diffraction (XRPD). The bulk chemical analysis of raw clays and mixtures (bricks) was performed by X-ray fluorescence (XRF) (we refer to Scott and Love, 1983, for ZAF correction and to Chen and Wang, 1988, for the standards used). Texture, mineral phases and vitrification level were studied under both optical microscopy and field emission scanning electron microscopy (FESEM) on polished thin sections. Hydric parameters (Tables S1, S2) of fired bricks were determined, and free and forced water absorption (UNI EN 13755, 2008), drying (NORMAL 29/88, 1988), capillarity rise (UNI EN 1925, 2000) calculated (Rilem, 1980; Cultrone et al., 2003). The ultrasound propagation velocity of compressional (Vp) and shear (Vs) pulses was measured in the three perpendicular directions on cubic samples (50-mm edge). Once the compressional and shear wave velocities had been determined, the Poisson coefficient (ν) and the Young (E), Shear (G) and Bulk (K) moduli, and the total (ΔM) and relative (Δm) anisotropies were calculated (Guydader and Denis, 1986) (Table S2). Uniaxial compressive strength of bricks was measured according to UNI EN 1926 (2007). Three cubic samples with 40-mm edges of each brick type were tested at a loading rate of 20 kg/s (Table S2). Accelerated aging tests were carried on three cubic samples (50-mm edge) per brick type, to evaluate their resistance to frost (UNI EN 12371, 2010) and salt crystallization (UNI EN 12370, 2001). At regular intervals of 5 cycles during the freeze-thaw test and 3 cycles of salt crystallization, sample compactness was also monitored by ultrasound.

Table 3
Mineralogical assemblages determined according to XRPD data of clay minerals. Mineral abbreviations: Qz = quartz; I = illite; Chl = chlorite; Kfs = K-feldspar; Pl = plagioclase; Cal = calcite; Dol = dolomite; Hem = Hematite. Relative quantity: **** = very abundant; *** = abundant; ** = medium; * = scarce; + = rare.

	Qz	I	Chl	Kfs	Pl	Cal	Dol	Hem
LGP	****	**	**	*	*	****	***	+
LRS	****	**	**	*	**	**	**	+
LRSS	****	**	**	**	**	*	*	+

3. Results

3.1. Raw clay materials and dye

Under chemical viewpoint (Table 2) clay LRSS is the richest in SiO_2 and LG the poorest; LG has the highest calcium and LOI, indicating that is rich in carbonate. On the basis of XRPD data, clay materials are mineralogically similar, but differ for the percentages of mineral phases (Table 3). Quartz, calcite, dolomite, feldspars *s.l.*, chlorite and illite occur in all samples. Comparisons of X-ray diffraction patterns confirm the higher carbonate content in LG than in the others, due to higher concentrations of calcite and dolomite. Quartz prevails in clay LRSS, followed by LRS. As regards clay minerals, illite and chlorite occur in all samples with weak reflections at 10.02 Å, and 13.99 and 6.99 Å, respectively, but being both more intense in LRS (Fig. 1). Parameters L*, a* and b* reveal some differences among the three clay materials (Table 4). In particular, GP, the most carbonate-rich, has the highest b* value, yellow component, and lightness. The dye additive, hausmannite, due to its mineralogical nature, is very different from the clay materials, with low L*, a* and b* tending to gray.

Table 2
Chemical composition of major elements expressed in wt% of oxides for clay materials (LG, LRS, LRSS) and bricks (GP, N, RS, RSS, R6). LOI = Lost on Ignition.

		SiO_2	Al_2O_3	Fe_2O_3	MnO	MgO	CaO	Na_2O	K_2O	TiO_2	P_2O_5	LOI
Clay	LG	39.81	10.63	3.87	0.08	4.75	17.76	0.54	2.37	0.43	0.11	19.65
	LRS	51.50	12.72	4.43	0.09	3.41	10.45	0.70	2.74	0.54	0.12	13.29
	LRSS	57.77	14.14	4.85	0.10	2.68	6.16	1.09	2.99	0.63	0.13	9.47
Fired bricks	GP (1050 °C)	50.17	13.19	4.80	0.09	5.61	20.39	0.72	2.84	0.49	0.13	1.56
	N (1050 °C)	42.41	11.67	4.93	12.86	4.93	17.63	0.60	2.66	0.52	0.15	1.63
	RS (980 °C)	59.46	14.53	4.94	0.09	3.69	11.06	0.89	2.99	0.59	0.13	1.62
	RSS (950 °C)	63.79	15.28	5.16	0.11	2.87	7.01	0.99	3.20	0.66	0.13	0.78
	R6 (600 °C)	60.32	14.35	4.85	0.11	2.69	6.22	0.93	3.03	0.64	0.13	6.74

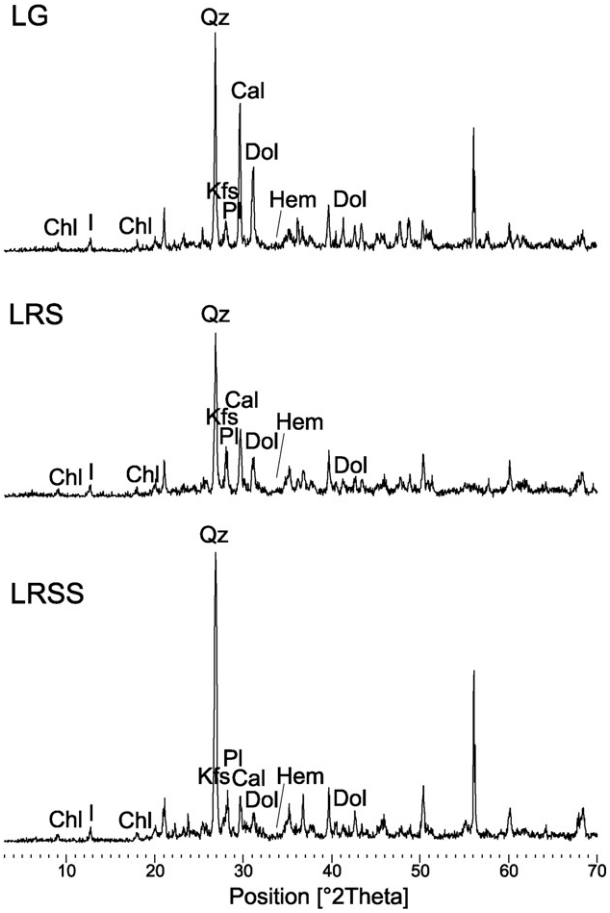

Fig. 1. XRPD patterns of clay materials (LG, LRS, LRSS).

3.2. Fired products

The colorimetry results of the fired bricks reflect those of the clay materials, with progressive increases in b* and lightness (L*) as the amount of carbonate increases (Table 4). The dye additive confers a dark color to sample N, with a*, b* and L* being the lowest. Samples R6 and RS show variations in color from the core (indicated by suffix –c) to the surface (indicated by suffix –s), due to non-homogeneous Fe oxidation during firing. In particular, R6 shows a darker core than the outer sides; the opposite, albeit far less evidently, is found in RS, with a lighter core. However, both samples show a decrease in a* (less marked in RS), perhaps due to a reduction in hematite and/or increase in magnetite, and visual appreciation of a lighter core in RS may be explained by a very slight increase in lightness. Samples N and GP are more sensitive to color changes after wetting, and both their a* and b* increase (Table 4). These changes can be seen more clearly in the total color difference ΔE values (Table 4). The color changes are usually below human perception limit, defined as ΔE ≥ 3 in the Lab color space (Benavente et al., 2002; Grossi et al., 2007b) and therefore invisible to the naked eye.

The chemical composition of the fired bricks obviously reflected that of the clay materials of which they are made, with differences in LOI in relation to firing temperature and to MnO wt% content in brick N. The higher LOI value (6.74 wt%) in R6 than in RSS (0.78 wt%) depends on the different firing temperatures, since the same clay was used to prepare both bricks. R6, fired at 600 °C, still contains calcite and dolomite phases which did not react (Table 3).

3.2.1. Mineralogy and texture

Under the optical microscope, bricks appeared texturally homogeneous. Inclusions were predominant sub-rounded grains of quartz and feldspar, varying in size up to 1 mm. The matrix of sample GP was the lightest, due to the higher content of carbonate in the raw materials (Fig 2a). Instead, sample N had a very dark aspect because of the presence of Mn oxides (Fig. 2b). Brownish Fe oxides were observed dispersed in the matrix (Fig. 2c), causing the red color in samples RSS, RS and R6, probably hematite, as the XRD results suggest. Phyllosilicates were also observed in RSS and R6 (Fig. 2d, e and f), both samples fired at lower temperature, allowing their typical optical behavior to be maintained.

The mineral composition of samples determined by XRPD analysis (Table 5) showed that RSS, RS, GP and N were composed of quartz, gehlenite, anorthite, sanidine and diopside, matching the high temperatures these samples reached during firing. The new phases were less abundant in RSS than in the other samples. Reflections of chlorite and illite were still present in R6 because of its low firing temperature (600 °C), due to reaction processes which were either weak or did not take place at all. These phases disappear when the firing temperature exceeds 900 °C (Cultrone et al., 2005b; Maritan et al., 2006), and this was confirmed by their absence in RSS, RS, GP and N.

As regards mineral transformations, calcite starts to react with illite to form gehlenite at 800–850 °C and with quartz to form Ca-rich silicates such as wollastonite at higher temperatures (900–1000 °C) (Duminuco et al., 1998; Riccardi et al., 1999), according to the following reactions:

$$1.2CaCO_3(\text{Calcite}) + 0.4KAl_4Si_7O_{20}(OH)_4(\text{illite}) \rightarrow 0.6Ca_2Al_2SiO_7(\text{Gehlenite}) + 0.4KAlSi_3O_8(\text{K-feldspar}) + 1.6H_2O + 1.2CO_2 \quad (1)$$

$$CaCO_3(\text{Calcite}) + SiO_2(\text{Quartz}) \rightarrow CaSiO_3(\text{Wollastonite}) + CO_2. \quad (2)$$

In addition, reactions occurring during firing are usually not stoichiometric (Cultrone et al., 2001a) and some of the chemical elements contribute toward forming the amorphous phase, the composition of

Table 4
Color coordinates, L*, a*, b* for raw clay and hausmannite additive (MN) and fired bricks, measured in dry and wet conditions and core (−c) and surface (−s) when differentiated. Also shown: color difference ΔE.

Raw materials				Fired bricks							
					Dry			Wet			ΔE
	L*	a*	b*		L*	a*	b*	L*	a*	b*	
LGP	63.89	2.41	16.05	GP	70.42	6.89	24.28	42.29	20.28	24.25	31.15
LRS	56.76	2.78	14.98	N	36.67	4.08	6.42	59.90	8.27	24.51	29.74
LRSS	57.74	4.07	17.97	RS-s	60.23	16.41	25.86	46.77	17.75	24.94	13.56
MN	35.67	10.85	8.70	RS-c	61.35	14.73	23.60	-	-	-	-
				RSS	56.51	19.05	25.40	44.53	20.22	24.37	12.08
				R6-s	54.79	14.92	25.58	38.85	17.19	22.82	16.34
				R6-c	53.51	9.35	20.01	37.80	10.51	17.36	-

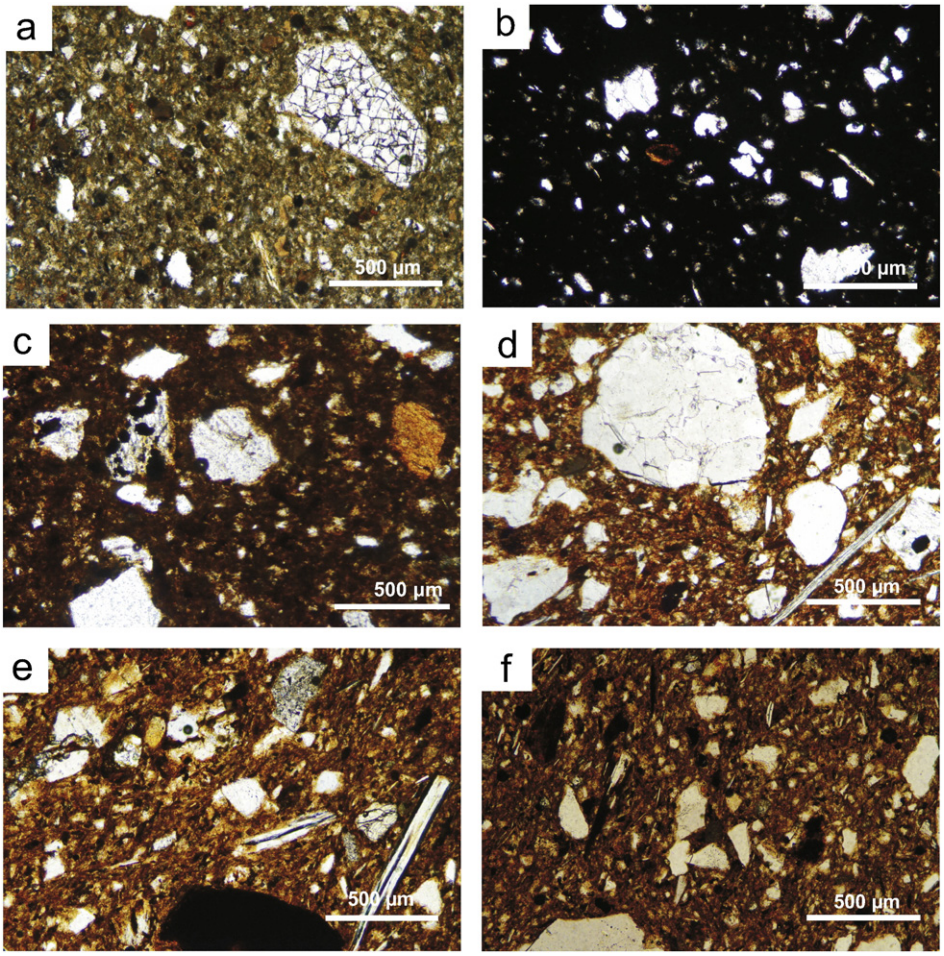

Fig. 2. Photomicrographs (plain polars) of fired bricks: a) light matrix and poorly sorted inclusion distribution, brick GP; b) quartz and feldspar in a dark matrix, brick N; c) Fe oxides on altered minerals and dispersed in a red matrix, brick RS; d) quartz crystals and phyllosilicate flakes in red matrix, brick RSS; e–f) sub-angular quartz crystals and phyllosilicate flakes in red matrix, brick R6.

which may be quite variable. Feldspars occurr in all samples but, although R6 contains orthoclase from the raw material, in the other bricks this feldspar is supposed to have changed to sanidine, the more stable high-temperature polymorph (Cultrone et al., 2001a). Plagioclase assumed anorthitic composition and in the temperature range 900–1050 °C diopside crystallized from dolomite and quartz (Cultrone et al., 2001a). Sample N is rich in bustamite ($CaMn(Si_2O_6)$), which developed from the reaction of hausmannite with calcite and quartz. Mn^{2+} cations from hausmannite partially substituted Ca^{2+} cations during the formation of the new silicate phase.

The diffractograms of GP and N showed higher background noise than the others because of the higher firing temperature, which caused the formation of an amorphous phase (Am; Table 5). The higher amorphous phase in N, produced with the same clay material and at the firing temperature of GP (1050 °C), depended on the addition of hausmannite, which acted as a fluxing agent, promoting the melting process.

High resolution FESEM analysis allowed both the study of brick textures and of the reaction rims between aplastic inclusions and the surrounding matrix to form new phases. As for the textural features, bricks differ greatly according to their firing temperature. In sample R6 (fired at 600 °C) the compactness is very low, clay raw materials are still evident in the groundmass, pores are irregular shaped (vughs), and the mineral inclusions are not bonded and have shrinkage rims (Fig. S1a). Bricks RSS and RS (fired at 950 °C and 980 °C, respectively) differ from the previous one (R6) by having a more compact matrix, due to the onset of sintering (Fig. S1b, c). In samples GP and N, fired at the highest temperature (1050 °C), the sintering effect is more evident (particularly in sample N), with inclusions which are almost completely decomposed or which reacted with the micromass; pores are less irregular (Fig. S1d, e).

As for the phase evolution, in brick R6, fired at 600 °C, only incipient dehydroxylation and decarbonation were observed. Phyllosilicates maintained their sheet-like fabric, although the loss of OH^- groups revealed exfoliation along basal layers. Carbonates were still recognizable, but secondary porosity appeared, due to the release of CO_2 from the crystals, as observed by Cultrone et al. (2014) in Ca-rich ceramics fired at low temperatures. Firing-induced transformation of feldspar is evident along preferential surfaces, like twinning and cleavage plains (Fig. 3a) and at the rims. No evidence of melting could be seen in the groundmass. In RS, fired at 980 °C, dehydroxylation was more extensive than in R6 and showed pseudomorphs of phyllosilicates (Fig. 3b).

Table 5
XRDP results: mineralogical assemblages in fired bricks. Mineral abbreviations: Qz = quartz; I = illite; Chl = chlorite; Kfs = K-feldspar; Pl = plagioclase; Cal = calcite; Dol = dolomite; Hem = hematite; Wo = wollastonite; Di = diopside; Gh = gehlenite; Bst = bustamite; Am = amorphous. Relative quantity: **** = very abundant; *** = abundant; ** = medium; * = scarce; + = rare; - = not detected.

	Qz	I	Chl	Kfs	Pl	Cal	Dol	Hem	Wo	Di	Gh	Bst	Am
GP (1050 °C)	****	-	-	**	*	-	-	*	**	***	***	-	**
N (1050 °C	****	-	-	**	*	-	-	*	**	***	***	***	***
RS (980 °C)	****	-	-	*	**	-	-	*	*	*	*	-	-
RSS (950 °C)	****	-	-	*	**	-	-	*	*	+	+	-	-
R6 (600 °C)	****	**	**	*	***	**	**	*	-	-	-	-	-

Dolomite and calcite were totally decomposed, with loss of CO_2, and Mg and Ca oxides reacted with silicates to form reaction rims along the borders of pre-existing carbonate grains. EDX analysis revealed the presence of wollastonite, growing close to quartz and calcite grains, with fibrous habit and nearly the same Ca:Si ratio (Fig. 3c). As regards brick RSS, fired at 950 °C, both textural features and mineralogical pattern were very similar to those of RS. Carbonates were completely decomposed and new phases had formed. Feldspar showed reaction rims with calcite, with progressive Ca enrichment (Fig. 3d). As spot analyses at the edges have shown, EDX spectra revealed several phases

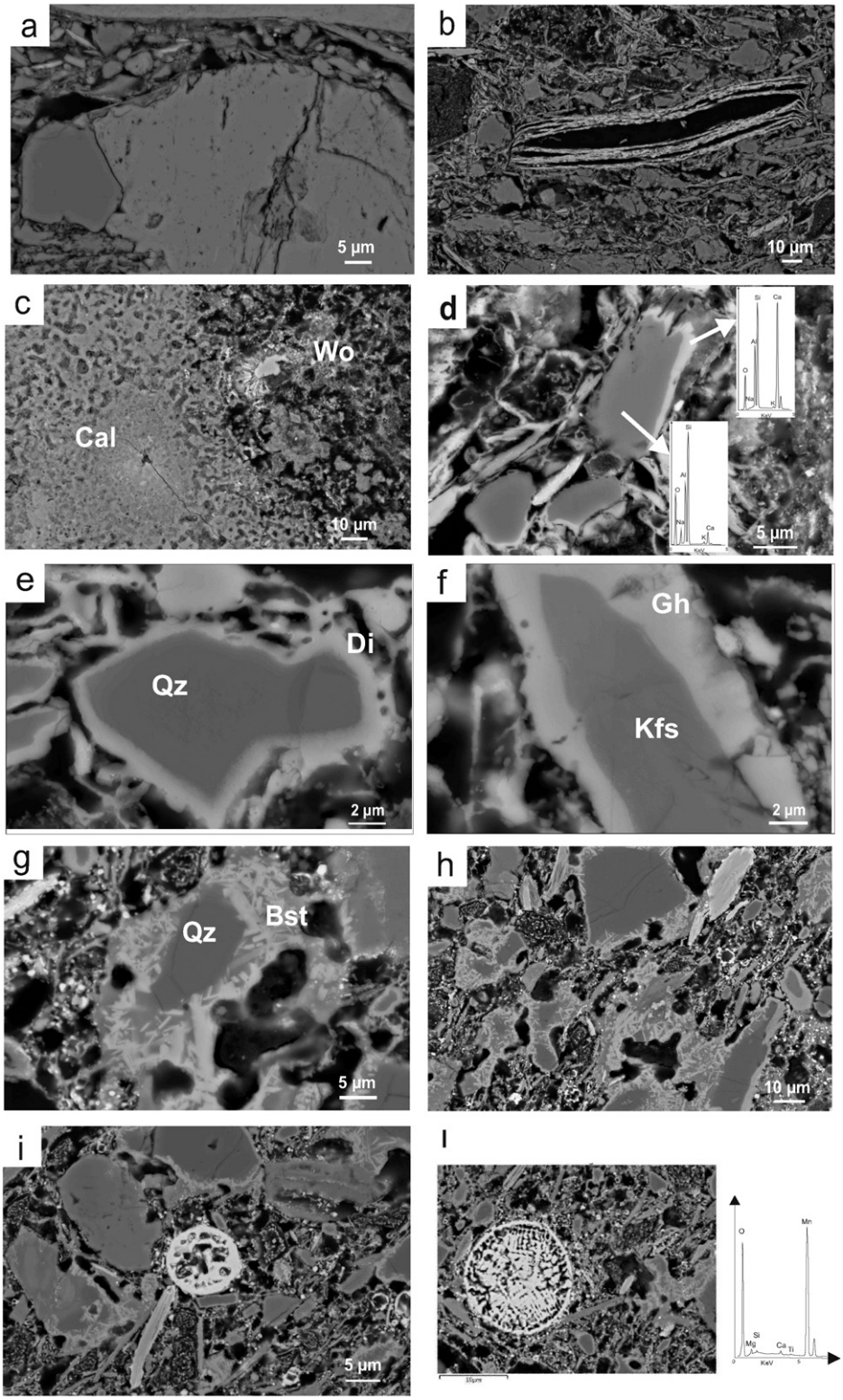

Fig. 3. FESEM-BSE images, some coupled with EDX spectra: a) development of along-cleavage fractures in feldspar grain and initial transformation of boundaries, brick R6; b) dehydroxylation of illite, brick R6; c) decarbonated calcite fragment in which wollastonite crystallized, brick RS; d) detail of the corona structure in a feldspar crystal with a rim enriched in Ca, where gehlenite was detected, brick RS; e) reaction rim on a quartz grain with formation of diopside, brick GP; f) reaction rim on a K-feldspar crystal and formation of gehlenite, brick GP; g) quartz grain with crystallization of bustamite (Bst), brick N; h) crystallization of bustamite at grain rims, brick N; i, l) presence of rounded aggregates of Mn oxides, brick N.

Table 6
Hydric parameters: A_b = free water absorption (%); A_f = forced water absorption (%); A_x = degree of pore interconnection (%); S = saturation coefficient (%); Di = drying index; p_{oHT} = open porosity; D_{bHT} = apparent density (kg m^{-3}); D_{skHT} = real skeletal density (kg m^{-3}); K_s = capillarity coefficient; B = capillarity rise. MIP values: p_{oMIP} = open porosity (%); D_{bMIP} = apparent density (kg m^{-3}); D_{skMIP} = real (skeletal) density (kg m^{-3}).

		GP	N	RS	RSS	R6
Hydric test	A_b	27.63	25.08	22.60	21.57	17.36
	A_f	28.71	25.85	23.09	23.28	17.88
	A_x	3.76	2.98	2.12	7.35	2.91
	S	96.26	97.00	97.33	92.47	96.13
	Di	1.35	1.36	1.36	1.37	1.37
	p_{oHT}	41.36	40.56	36.75	37.52	31.14
	d_{bHT}	1.44	1.57	1.58	1.61	1.72
	d_{skHT}	2.46	2.64	2.50	2.57	2.50
	Ks	0.43	0.33	0.32	0.30	0.16
	B	1.33	1.23	1.21	1.29	0.72
MIP	p_{oMIP}	47.45	46.87	42.25	38.84	34.27
	d_{bMIP}	1.40	1.50	1.54	1.54	1.70
	d_{skMIP}	2.68	2.87	2.66	2.55	2.58

with non-stoichiometric composition, due to sub-solidus reactions, with a passage to gehlenite (spectra of Fig. 3d), as also attested by XRPD data. Bricks GP and N (fired at 1050 °C) showed a partially vitreous groundmass and well-developed reaction bridges, especially along quartz and feldspar borders. At 1050 °C, phyllosilicates were completely dehydroxylated. Firing had transformed the structure, giving rise to abundant secondary bubbles and Fe-bearing oxides. Grains of quartz and K-feldspar showed evident transformations at the rims, diopside preferentially nucleating at quartz rims (Fig. 3e) and gehlenite at K-feldspar rims (Fig. 3f). Brick N was characterized by the presence of bustamite, a Mn-rich wollastonite, also observed by XRPD, diffused along most of the reacted boundaries (Fig. 3g and h). Many large rounded mineral aggregates were also observed in the matrix, with diameters ranging between 10 and 50 μm, sometimes with dendritic patterns (Fig. 3i and l). EDX analysis of these grains revealed Mn and O (sometimes with a little Fe), indicating that they are Mn oxides deriving from hausmannite, partially melted at 1050 °C.

3.2.2. Water behavior and pore system

The hydric parameters of fired samples are listed in Table 6 and shown in Fig. 4. GP was the brick with the highest free and forced absorption values (A_b = 27.63%, A_f = 28.71%, respectively). N, RS and RSS samples showed intermediate values, whereas R6 stood out for its low capacity to absorb water (A_b = 17.36%, A_f = 17.88%).

RS showed the best pore interconnections (A_x = 2.12%), followed by R6 and N. RSS had the highest value (A_x = 7.35%), indicating the presence of pores with little access to water. However, all samples dried within 200 h, had similar drying curves (Fig. 4a), and their drying indexes were all very similar. GP had the lowest drying index (Di = 1.35); R6 had the slowest water release (Di = 1.37) (Table 6). Saturation coefficient (S) was >90% for all bricks, confirming good water absorption behavior. The percentage of open porosity (p_o) follows the extent of carbonate content of the samples. GP and N, the most carbonatic bricks, had the highest values of open porosity (41.36% and 40.56%, respectively), RSS and RS were intermediate (37.52%, 36.75%) and R6 was the lowest (31.14%). The results of the capillarity test highlighted the trend followed by the free water absorption (Table 6). Sample GP had a capillarity rise of 0.43; R6 had the lowest value (Ks = 0.16); and N, RS and RSS were intermediate. Capillarity is an important parameter as regards brick durability, and this behavior suggests that GP is the brick most sensitive to deterioration. This confirms the close relation between firing temperature, pore system and water absorption behavior. In general, samples fired at lower temperatures have smaller pores and lower capillarity rise, whereas at higher temperatures the pore system develops rounder and larger pores, with a consequent tendency to absorb more water (Benavente et al., 2006).

Table 7
Ultrasonic test. Propagation velocities of ultrasonic Vp and Vs pulses (m s^{-1}). ΔM = total anisotropy (%); ν = Poisson's ratio; E = Young's modulus (GPa); G = shear modulus (GPa); K = bulk modulus (GPa). Uniaxial test: σ = stress values (kg cm^{-2}).

	GP	N	RS	RSS	R6
Vp	2773	2804	2272	1857	1441
Vs	1299	1299	1106	893	752
ΔM	12.26	10.73	14.26	18.07	20.38
Δm	2.66	1.31	1.59	4.96	0.91
ν	0.36	0.45	0.34	0.35	0.31
E	64.20	68.78	70.10	50.63	25.22
G	9.02	9.39	10.54	7.86	4.71
K	76.19	83.96	77.68	54.36	22.49
σ	151	191	156	126	71

3.2.3. Compactness and durability

The highest velocity values (Vp and Vs) were measured in bricks GP and N (Table 7), and the lowest ones in R6, the former being the most compact bricks, and the latter the least. The highest total anisotropy value (ΔM) was observed in R6. Its low compactness and high anisotropy is explained by the absence of a melting process in the matrix (or its delevolpment at incipient stage), and the presence of preferentially oriented phyllosilicates (Cultrone et al., 2005a). With increasing firing temperature, as in GP and N, texture became more homogeneous. Poisson's ratio (ν) values were very similar in all the bricks, with a small rise in samples rich in calcite. Ji et al. (2009) and Cultrone et al. (2012) have observed that calcite content and Poisson's ratio (ν) are directly correlated: an increase in calcite raises Poisson's ratio. RS stands out for the highest Young (E) and Shear moduli (G) (E = 70.1 GPa and G = 10.54 GPa), whereas the highest bulk modulus value (K) was measured in N (K = 83.96 GPa), followed by RS (K = 77.68 GPa). At the other extreme, R6 showed the lowest values with great differences (E = 25.22 GPa, G = 4.71 GPa and K = 22.49 GPa) (Table 7). In bricks fired at temperatures above 950 °C, melting and formation of new silicate phases take place, contributing to the improvement of the mechanical features; at 600 °C (sample R6) these transformations did not take place yet or are at an initial stage. In addition, the fact that the

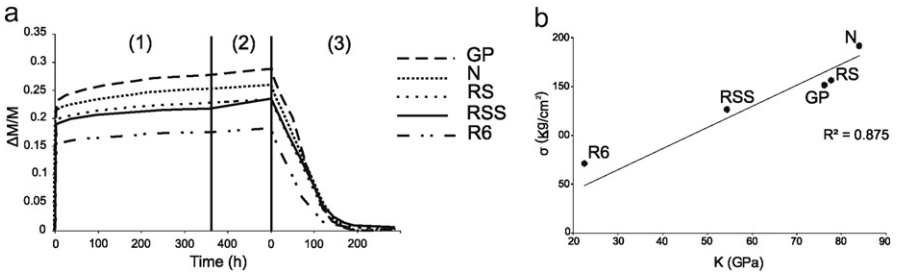

Fig. 4. a) Results of hydric test: free water absorption (1), forced water absorption (2) and drying (3) of bricks GP, N, RS, RSS and R6. Weight variation (ΔM/M) vs. time (h); b) comparison of bulk modulus values, K (GPa), obtained from ultrasound measurements and stress values, σ (kg cm^{-2}), measured with uniaxial compressive test.

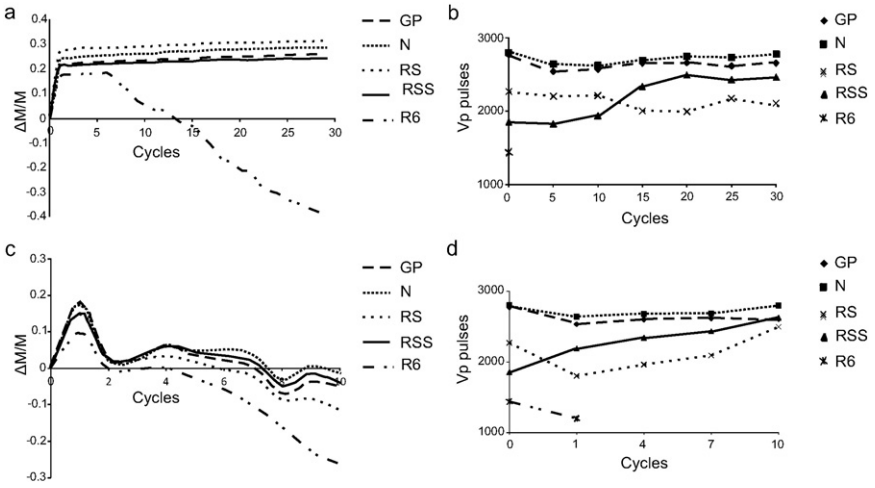

Fig. 5. a) Weight variation (ΔM/M) vs. time (h) of bricks GP, N, RS, RSS and R6 subjected 30 freeze-thaw cycles; b) propagation velocities of ultrasonic Vp pulses (m s^{-1}) during freeze-thaw test; c) weight variation (ΔM/M) vs. time (h) of bricks GP, N, RS, RSS and R6 subjected to 10 salt crystallization cycles; d) propagation velocities of ultrasonic Vp pulses (m s^{-1}) during salt crystallization test.

mechanical properties and the total anisotropy of brick N are different from those of GP, although both have the same composition and firing temperature, suggests that addition of the dye hausmannite increases the vitrification level and, therefore, the mechanical properties of N. This trend was confirmed by the mechanical stress values (σ) measured through the uniaxial compressive test. The highest σ value was measured in N (σ = 191 kg cm^{-2}), followed by GP and RS with similar resistances (151 and 156 kg cm^{-2}), by RSS (σ = 126 kg cm^{-2}) and a much lower value in R6 (σ = 71 kg cm^{-2}). When the average results of mechanical parameters obtained by the ultrasound test (bulk modulus, K) were compared with those of the uniaxial compressive test (stress values, σ), quite good agreement was observed (Fig. 4b).

As regards durability, data from freeze-thaw tests showed similar initial behavior in all bricks: after the first cycle, RS had the greatest variation in weight increase, followed by N, GP, RSS and R6 (Fig. 5a). Until the seventh cycle, there was a constant weight increase in all samples. Then the curve of R6 dropped rapidly and, at the end of the test, its weight loss value was around 52%. The poor durability of R6 could easily be observed by the naked eye, with a gradual loss of fragments. Flaking began with fragments of about 0.5 mm, followed by generalized extensive powdering. The development of fissures and cracks was confirmed by the absence of ultrasonic wave transmission already at the fifth cycle. As regards the other bricks, GP and N were very similar and did not show particular changes, only small oscillations (Fig. 5b).

The salt crystallization test caused damage, mainly along brick edges. In all bricks, a weight increase also occurred at the beginning of the test, caused by the entry of salt crystals into pores and fissures (Fig. 5c). In R6, the tendency to salt damage was detected by the fall in the weight variation diagram (Fig. 5c) and the absence of wave transmission at the first ultrasound measurement (after the first cycle) due to the development of internal fissures (Fig. 5d). The other bricks had similar trends: the weight loss of dried samples after 10 cycles of salt crystallization was the highest in R6 (~30%) and the lowest in N (~10%); the values for the other samples ranged between 12% and 17%. Ultrasound showed similar behavior in N, GP and RS, all characterized by a slight decrease in velocity in the first cycles and a subsequent increase in their initial values; in RSS, wave velocity remained constant. The increased velocity during the deterioration test was due to salt crystals in fissures, which allowed faster transmission of pulses.

4. Conclusions

The multianalytical approach adopted to studying SanMarco-Terreal bricks fired at 600, 950, 980 and 1050 °C highlights close relationships among mineralogy, porosity and physical properties and their behavior in varying stress environments.

The important role of firing on the characteristics of the final products is clear-cut. In the sample fired at the lowest temperature (R6), the absence of new silicates and interconnections due to melting made it the weakest in load resistance and decay tests. This implies that this sample, produced experimentally but not actually marketed, does not reach standard requirements of durability and load resistance. Conversely, samples fired at the highest temperature 1050 °C, GP and N) responded well to stress, but tended to absorb more water. Brick fired at lower temperature (980 °C, RS) exhibited the best compromise in physical-mechanical properties, decay and water behavior. Therefore, the latter sample represents a good-quality brick obtained at a lower firing temperature, thus reducing energy consumption and production costs. These results make a valuable contribution to the development of brick production and the improved quality of final products, to aim at new ad hoc mix designs and to face the new challenges in a sustainable and compatible industry.

Supplementary data to this article can be found online at http://dx.doi.org/10.1016/j.clay.2016.02.014.

Acknowledgments

This study was funded by Research Group RNM179 of the *Junta de Andalucía* and by Research Project MAT2012-34473. The research benefitted by funding from INPS - *Gestione Ex Inpdap* (*Direzione Regionale Veneto*), which provided the PhD "Doctor J" Grant over the period 2012-2015. The authors are grateful to Gabriel Walton who revised the English test, and to Emilio Galán and one anonymous referee, whose comments improved the manuscript.

References

Anzani, A., Binda, L., Carpinteri, A., Invernizzi, S., 2010. A multilevel approach for the damage assessment of historic masonry towers. J. Cult. Herit. 11, 459–470.
Aras, A., 2004. The change of phase composition in kaolinite- and illite-rich clay-based ceramic bodies. Appl. Clay Sci. 24, 257–269.
Benavente, D., Martiñez-Verdú, F., Bernabeu, A., Viqueira, V., Fort, R., García del Cura, M.A., Illueca, C., Ordóñez, S., 2002. Influence of surface roughness on color changes in building stones. Color. Res. Appl. 28, 343–351.
Benavente, D., García del Cura, M.A., Ordoñez, S., 2003. Salt influence on evaporation from porous building rocks. Constr. Build. Mater. 17, 113–122.
Benavente, D., Linares-Fernández, L., Cultrone, G., Sebastián, E., 2006. Influence of microstructure on the resistance to salt crystallization damage in bricks. Mater. Struct. 39, 105–113.

Cardiano, P., Ioppolo, S., De Stefano, C., Pettiganno, A., Sergi, S., Piraino, P., 2004. Study and characterization of the ancient bricks of monastery of "San Filippo di Fragalà" in Frazzanò (Sicily). Anal. Chim. Acta 519, 103–111.
Carretero, M.I., Dondi, M., Fabbri, B., Raimondo, M., 2002. The influence of shaping and firing technology on ceramic properties of calcareous and non-calcareous illitic–chloritic clays. Appl. Clay Sci. 20, 301–306.
Chen, G., Wang, J., 1998. The preparation of marine geological certified reference materials - Polymetallic nodule GSPN-1 and marine sediment GSMS-1 from the Central Pacific Ocean. Geostandards and Geoanalytical Research 22, 119–125.
Cultrone, G., Sebastián, E., 2009. Fly ash addition in clayey materials to improve the quality of solid bricks. Constr. Build. Mater. 23, 1174–1184.
Cultrone, G., de La Torre, M.J., Sebastián, E., Cazalla, O., Rodriguez-Navarro, C., 2000. Behaviour of brick samples in aggressive environments. Water Air Soil Pollut. 119, 191–207.
Cultrone, G., Rodriguez-Navarro, C., Sebastián, E.M., Cazalla, O., de la Torre, M.J., 2001a. Carbonate and silicate phase reactions during ceramic firing. Eur. J. Mineral. 13, 621–634.
Cultrone, G., Sebastián, E., Cazalla, O., Nechar, M., Romero, R., Bagur, M.G., 2001b. Ultrasound and mechanical tests combined with ANOVA to evaluate brick quality. Ceram. Int. 27, 401–406.
Cultrone, G., de la Torre, M.J., Sebastian, E., Cazalla, O., 2003. Evaluación de la durabilidad de ladrillos mediante tecnicas destructivas (TD) y no-destructivas (TND). Mater. Constr. 53, 41–59.
Cultrone, G., Sebastián, E., Elert, K., de la Torre, M.J., Cazalla, O., Rodriguez-Navarro, C., 2004. Influence of mineralogy and firing temperature in the porosity of bricks. J. Eur. Ceram. Soc. 34, 547–564.
Cultrone, G., Sidraba, I., Sebastián, E., 2005a. Mineralogical and physical characterization of the bricks used in the construction of the "Triangul Bastion", Riga (Latvia). Appl. Clay Sci. 28, 295–308.
Cultrone, G., Sebastián, E., de la Torre, M.J., 2005b. Mineralogical and physical behaviours of solid bricks with additives. Constr. Build. Mater. 19, 39–48.
Cultrone, G., Sebastián, E., Ortega, Huertas M., 2007. Durability of masonry systems: a laboratory study. Constr. Build. Mater. 21, 40–51.
Cultrone, G., Luque, A., Sebastián, E., 2012. Petrophysical and durability tests on sedimentary stones to evaluate their quality as building materials. Q. J. Eng. Geol. Hydrogeol. 45, 415–422.
Cultrone, G., Molina, E., Arizzi, A., 2014. The combined use of petrographic, chemical and physical techniques to define the technological features of Iberian ceramics from the Canto Tortoso area (Granada, Spain). Ceram. Int. 40, 10803–10816.
De Bonis, A., Cultrone, G., Grifa, C., Langella, A., Morra, V., 2014. Clays from the bay of Naples (Italy): new insight on ancient and traditional ceramics. J. Eur. Ceram. Soc. 34, 3229–3244.
Dondi, M., Ercolani, G., Fabbri, B., Marsigli, M., 1998. An approach to the chemistry of pyroxenes formed during the firing of Ca-rich silicate ceramics. Clay Miner. 33, 443–452.
Ducman, V., Škapin, S.A., Radeka, M., Rnogajec, J., 2011. Frost resistance of clay roofing titles: case study. Ceram. Int. 37, 85–91.
Duminuco, P., Messiga, B., Riccardi, M.P., 1998. Firinig process of natural clays. Some microtextures and related phase compositions. Termodicnamica Acta 321, 185–190.
Elert, K., Cultrone, G., Rodriguez, Navarro C., Sebastián, Pardo E., 2003. Durability of bricks used in the conservation of historic buildings — influence of composition and microstructure. J. Cult. Herit. 4, 91–99.
Eliche-Quesada, D., Martínez-Martínez, S., Pérez-Villarejo, L., Iglesias-Godino, F.J., Martínez-García, C., Corpas-Iglesias, F.A., 2012. Valorization of biodiesel production residues in making porous clay brick. Fuel Process. Technol. 103, 166–173.
Fabbri, B., Gualtieri, S., Shoval, S., 2014. The presence of calcite in archaeological ceramics. J. Eur. Ceram. Soc. 34, 1899–1911.
Grossi, C.M., Brimblecombe, P., Harris, I., 2007a. Predicting long term freeze-thaw risks on Europe built heritage and archaeological sites in a changing climate. Sci. Total Environ. 377, 273–281.
Grossi, C.M., Brimblecombe, P., Esbert, R.M., 2007b. Francisco Javier Alonso. Color changes in architectural limestones from pollution and cleaning. Color. Res. Appl. 32, 320–331.
Guydader, J., Denis, A., 1986. Propagation des ondes dans les roches anisotropes sous contrainte évaluation de la qualité des schistes ardoisiers. Bull. Int. Assoc. Eng. Geol. 33, 49–55.
Ji, S., WAng, Q., Salisbury, M.H., 2009. Composition and tectonic evolution of the Chinese continental crust constrained by Poisson's ratio. Tectonophysics 463, 15–30.
Larbi, J.A., 2004. Microscopy applied to the diagnosis of the deterioration of brick masonry. Constr. Build. Mater. 18, 299–307.
López-Arce, P., García-Guinea, J., Gracía, M., Obis, J., 2003. Bricks in historical buildings of Toledo City: characterisation and restoration. Mater. Charact. 50, 59–68.
Maritan, L., Mazzoli, C., Nodari, L., Russo, U., 2005. Second Iron Age grey pottery from Este (northeastern Italy): study of provenance and technology. Appl. Clay Sci. 29, 31–44.
Maritan, L., Nodari, L., Mazzoli, C., Milano, A., Russo, U., 2006. Influence of firing conditions in ceramic products: experimental study on clay rich in organic matter. Appl. Clay Sci. 31, 1–15.
Monteiro, S.N., Fontes Vieria, C.M., 2014. On the production of fired clay bricks from waste materials: a critical update. Constr. Build. Mater. 68, 310–599.
Nodari, L., Marcuz, E., Maritan, L., Mazzoli, C., Russo, U., 2007. Hematite nucleation and growth in the firing of carbonate-rich clay for pottery production. J. Eur. Ceram. Soc. 27, 4665–4673.
Normal 29/88, 1988. Misura dell'indice di asciugamento (drying index). CNR-ICR, Rome.
Riccardi, M.P., Messiga, B., Duminuco, P., 1999. An approach to the dynamics of clay firing. Appl. Clay Sci. 15, 393–409.
RILEM, 1980. Recommended test to measure the deterioration of stone and to assess the differences of treatment methods. Mater. Struct. 13, 175–253.
Rodriguez-Navarro, C., Doehne, E., Sebastián, E., 2000. How does sodium sulfate crystallize? Implications for the decay and testing of building materials. Cem. Concr. Res. 30, 1527–1534.
Scott, V.D., Love, G., 1983. Quantitative Electron Probe Microanalysis. John Wiley and Sons, New York.
Setti, M., Lanfranchi, A., Cultrone, G., Marinoni, L., 2012. Archeometric investigation and evaluation of the decay of ceramic materials from the Church of Santa Maria del Carmine (Pavia, Italy). Materiales de Costrucción 62 (305), 79–98.
UNE EN 15886, 2011. Conservación del patrimonio cultural. Métodos de ensayo. Medición del color de superficies. A.E.N.O.R., Madrid.
UNI EN 12370, 2001. Natural stone test methods - Determination of resistance to salt crystallisation. CNR-ICR, Rome.
UNI EN 12371, 2010. Natural stone test methods - Determination of frost resistance. CNR-ICR, Rome.
UNI EN 13755, 2008. Natural stone test methods - Determination of water absorption at atmospheric pressure. CNR-ICR, Rome.
UNI EN 1925, 2000. Natural stone test methods - Determination of water absorption coefficient by capillarity. CNR-ICR, Rome.
UNI EN 1926, 2007. Natural stone test methods - Determination of uniaxial compressive strength. ICNR-ICR, Rome.
Valluzzi, M.R., Bondì, A., da Porto, F., Franchetti, P., Modena, C., 2002. Structural investigations and analyses for the conservation of the 'Arsenale' of Venice. J. Cult. Herit. 3, 65–71.
Valluzzi, M.R., Binda, L., Modena, C., 2005. Mechanical behaviour of historic masonry structures strengthened by bed joints structural repointing. Constr. Build. Mater. 19, 63–73.
Zhang, L., 2013. Production of bricks from waste materials — a review. Constr. Build. Mater. 47, 643–655.